

Spectral characteristics of infrared radiation from forest fires

Han Sun^{*a}, Zhiguo Rong^a, Cheng Liu^a, Jingjing Liu^a, Yan Zhang^a, Peng Zhang^a, Xinli Wang^b, and Wei Gao^b

^aRemote Sensing Application and Experiment Station, National Satellite Meteorological Center,
Nanning, Guangxi Province, China;

^bUSDA UV-B Monitoring and Research Program, Natural Resource Ecology Laboratory,
Colorado State University, Fort Collins, USA

ABSTRACT

Field experiments with man-made fires in a forest were conducted to verify fire warning products from satellite remote sensing techniques and to select more effective channels for producing these products. Pine branches and trunks as well as other woods were burned at a designated place in a pine-dominated forest to simulate wild forest fires when a satellite was passing over the sky. Infrared spectral irradiances, visible spectrum, brightness, and temperature were measured concurrently with satellite data at the ground using a medium and near-infrared MOMEM MR154 FT-Spectroradiometer, an infrared thermal imager, and a visible and near-infrared spectroradiometer (ASD FR). The measurements showed two emission peaks in middle infrared band that corresponded exceptionally to the combustion strength. One of the spikes at 4.17 μm reflected the CO emission peak. The other peak spanned through the wavelengths of 4.34-4.76 μm , which exhibited a much stronger response to the fire than the commonly used channel 3.5-4.0 μm for fire monitoring in remote sensing. The results suggest that the wave band 4.34-4.76 μm is probably more sensitive and more effective than the common-used channel for wild fire monitoring using satellite remote sensing techniques. However, the peak of this wavelength band drifted during the burning process, which should be taken into account in channel selection. This band is suitable to determine forest fires. Further studies are needed to use it for retrieving fire strength quantitatively.

1. INTRODUCTION

The National Satellite Meteorological Center (NSMC) of the China Meteorological Administration initiated a project in 1985 to use NOAA satellite data in monitoring forest fires. For the first time, a fire was observed at the grassland in Inner Mongolia on April 13th, 1986. The NSMC began to provide the Fireproofing Headquarters of Forest Management, China, with the information of forest fires monitored by using meteorological satellite data in the fall of 1986. In May, 1987, a strong forest fire, which was unusual since the foundation of the People's Republic of China, occurred in Daxinganling forest region in northeastern China. During the fire fighting, the NSMC provided systematic monitoring services of the fire development and contributed much useful fire monitoring information from satellite remote sensing data to the State Council of China, Firefighting Frontline Headquarters, and related departments in the China Meteorological Administration.

The current technique for fire monitoring by satellite remote sensing is based the data from middle infrared channel (3.5-4.0 μm) and far infrared channel (10.5-12.5 μm) or from two split windows (10.3-11.3 μm , 11.5-12.5 μm). Burning objects are separated from the background scene through processing these data. Fire spots can be identified through a series of estimations and recognitions. However, the resolution of the infrared channel is only 1 km in meteorological satellites and environmental satellites. The actual size of most burning areas (fire spots) is usually less than 1 km², especially at the beginning of the fire. Sub-pixel models have been developed to derive fire information from satellite data for determining the size, strength and the temperature of observed fire. The products can then be provided for use in fire fighting. Dozier proposed the theory of surface temperature field of sub-pixel resolution¹. A technique was also developed by Dozier to process AVHRR data for fire identification. Currently, sub-pixel models are still a basic technique to detect and analyze information in fire monitoring²⁻⁴. Yet, it is very difficult to apply this technique in professional services for precise and quantitative fire monitoring.

With the advances in remote sensing quantitative technology of operational meteorological satellite in China (FY-1C, FY-1D, and FY-2C), it is imperative to validate the quantitative products of remote sensing. It is critical and essential to

* Corresponding author, sun_han@163.com; phone: 86-771-5852120; Remote Sensing Application and Experiment Station of National Satellite Meteorological Center, 81 Minzu Street, Nanning, Guangxi Province 530022, People's Republic of China.

quantitatively investigate the characteristics of the micro-structure of remote sensing products, including those for fire monitoring.

In order to verify the fire monitoring products and to analyze the sensitivity of meteorological satellites in detecting high-temperature targets (the minimum area of a fire), we performed synchronous measurement experiments of man-made fires and satellites near the Sporting Airport of Wuming County, Guangxi Province, China, in October 2005. Infrared spectral irradiances, brightness, temperature, and visible spectral irradiances were measured synchronously while a satellite was passing over. In this paper, we will give the design of the experiments, provide the calibration method of BOMEM MR154 FT-Spectroradiometer, introduce the approaches to carry out the measurements, present the observed facts, and discuss the application prospects of our results.

2. EXPERIMENT DESIGN

2.1 Time selection

Fall is a good season for the experiment since it is the season when wild fires happen most frequently. The actual time for the experiments is determined by many factors, including the time when the satellite is passing over, weather condition, and if preparation is sufficient. The experiments in this study were performed during the last ten days in October, 2005. The actual times were on 20th, around 23:04 Beijing time while the satellite EOS-TERRA was passing over, on 23rd, around 19:59 Beijing time while the satellite FY-1D was passing over, and 28th, around 11:20 Beijing time while the satellite NOAA-17 was passing over. These were clear sky days.

2.2 Man-made fires

The area of the fire, the geometric shape of the burning area, and the materials to burn to make the fire are the three components to be considered when a fire is made. The size is determined by the minimum area of a fire the NOAA and FY-1D satellites can detect. In the first experiment, the area was 100m². The areas in the last two experiments were 200m² in the consideration that this spot could be split or stretched into two pixels. To avoid the effects of orientation, a circular fire spot was set in all three experiments. Pine branches and other woods were burned to make the fire. In addition, pine trunks were set upright in the fire to simulate a forest fire (Figure 1).



Figure 1 An example of the fire, night of October 20th, 2005.

2.3 Instruments and measurements

Instruments and equipments used in the experiments include thermal imager, BOMEM MR154 FT-Spectroradiometer, thermometer for high temperature, CE-312 thermal-infrared radiometer, ASD FieldSpec FR Spectroradiometer, SONY optical digital professional camera, automatic sun tracking photometer CE318, ground weather station, meteorological sounder, unmanned aircraft, and a operational cart of 20 m. The cart was located out of the directions of $\pm 30^\circ$ relative to the west to avoid the situation in which the cart and the fire were in the same scan line. The measurement heights on the

cart were at 1.5, 2.5, 5, 10, 15, and 17.5 meters above the ground. The thermal imager was set at 50 m away from the fire in the upwind direction and 17.5 m above the ground. The BOMEM MR154 FT-Spectroradiometer was set at the same location as the thermal imager, but at 1.5 m above the ground. At the same location, also set were the thermometer for high temperatures, an optical digital professional camera, a CE-312 thermal-infrared radiometer at 2.5 m above the ground, and an ASD FieldSpec FR Spectroradiometer at 2.5m above the ground. Clocks of the instruments were all synchronized with the GPS time.

Synchronous measurements with satellite data were infrared spectral irradiances, visible spectral irradiances, brightness, temperature, and photograph pictures from the fires. In addition, spectral irradiance measurements were also made from several man-made fires with the areas of 10m², 20m², and 40m².

At the beginning, background spectral irradiances were measured by the thermal imager and the BOMEM spectroradiometer. The thermal imager was recorded every 2 seconds and the spectroradiometer was recorded every 30-60 seconds. When the fire was up and stabilized, measurements of thermal imager and spectroradiometer were made at 2.5, 5, 10, 15, and 17.5 meters downward to the fire in turn with the resort to the operational cart. First, the spectroradiometer was placed at 1.5 m to make measurements continuously and measurements of the imager were made at those heights, 20 seconds at each height and recording every 2 seconds. Then the imager was collocated with the spectroradiometer and synchronous measurements were taken for 20 seconds. Afterwards, the imager remained at 1.5 m and the spectroradiometer was set on the operational cart to make measurements at the same heights. When these measurements were done, the spectroradiometer was collocated with the imager again for synchronous measurements. When this cycle was finished, the operational cart was relocated at 100 m away from the fire in the same direction and the same measurements were made as above. These observations were repeated until the fire ceased.

The measurements of the thermometer were made in the same direction as the thermal imager. The location and time were also recorded for each measurement. Temperatures during the experiment were measured by the CE-312 thermal-infrared radiometer. Reflection was measured by the ASD FieldSpec FR Spectroradiometer. A video of the fire was made using an optical digital video recorder. Optical depths of the atmosphere were measured with the automatic sun tracking photometer CE-318. Concurrent ground meteorological observations were made at the ground weather station. Synchronous atmospheric sounding was made with a sounding system. Photographs of the fire were taken from the unmanned aircraft in the atmosphere.

3. BOMEM MR154 FT-SPECTRORADIOMETER AND ITS CALIBRATION

3.1 The BOMEM MR154 FT-Spectroradiometer

The BOMEM MR-154 FT-Spectroradiometer is one of the Bomem's 100-series products. Its optical system comprises of a Michelson interference device. Bomem MR154 is equipped with an infrared detector MCT (mercury cadmium tellurium TeCdHg) (2-20μm, 5000-500cm⁻¹), a short-wave infrared detector (InSb antimony, indium; 1.1-5.5μm, 9090-1818cm⁻¹), and one near-infrared detector (Si silicon; 0.7-1.17μm, 14285-8547cm⁻¹). In this study, we used MCT detector. The highest resolution of MR154 is 1 cm⁻¹.

3.2 The calibration principle

The spectral radiance is given by the Plank function:

$$L(\sigma) = \frac{C_1 \sigma^3}{\exp\left(\frac{C_2 \sigma}{T}\right) - 1}, \quad (1)$$

where $C_1 = 1.191 \times 10^{-12}$ W/(cm²sr(cm⁻¹)⁴), $C_2 = 1.439$ °Kcm, σ is the wave number in cm⁻¹, T is temperature in °K, and $L(\sigma)$ is spectral radiance in W/cm² sr cm⁻¹.

An ideal radiometer is linear. The signal from each channel is proportional to the irradiance from measured target. The observed radiative power includes the power from the targeted object and the thermal radiation from the instrument. As a result, characteristic measurements (system calibration) must be made at least at two points and the line connecting these two points does not pass the origin since the thermal radiation from the instrument cannot be ignored.

A measurement for calibration can be expressed as follows:

$$S^{Measured}(\sigma) = K(\sigma)(L^{Source}(\sigma) + M^{Stray}(\sigma)). \quad (2)$$

Where $S^{Measured}(\sigma)$ is the measured complex original spectrum (arbitrary), $K(\sigma)$ is the complex instrument response function, $L^{Source}(\sigma)$ is the spectral irradiance from the target, and $M^{Stray}(\sigma)$ is the spectral stray irradiance.

The interference gram has a certain asymmetry due to the dispersion of beam splitter (the refraction index of different wavelengths) and the errors at different amplification stages (the frequency-dependent electronic delay). This asymmetry results the imaginary value in the Fourier transformation of interference gram (spectrum). Due to its special design, the calibration of this instrument can be done by using the complex spectrum directly, instead of separating real part from the complex spectrum.

There are two steps in the calibration. The first is to determine the gain, $K(\sigma)$, and the offset, $M^{Stray}(\sigma)$, of the sensor. The second is to calculate the calibration spectrum of an uncalibrated measurement.

Two measurements, a hot blackbody measurement (with a temperature higher than target) and a cold blackbody measurement (with a temperature lower than target), are needed to determine the gain and the offset. With these two measurements, the irradiance of targeted blackbody is deduced through Equations (3) and (4), where $L_H(\sigma)$ and $L_C(\sigma)$ are the spectral irradiances of the measured blackbodies.

$$L_H(\sigma) = S_H^{Measured}(\sigma) / K(\sigma) - M^{Stray}(\sigma), \quad (3)$$

$$L_C(\sigma) = S_C^{Measured}(\sigma) / K(\sigma) - M^{Stray}(\sigma). \quad (4)$$

In Equation (5), x is equal to C for a cold blackbody and to H for a hot blackbody, $\varepsilon_x(\sigma)$ is the emissivity of blackbody x , and T_x is the temperature of blackbody x .

$$L_x(\sigma) = \varepsilon_x(\sigma) \frac{C_1 \sigma^3}{\exp\left(\frac{C_2 \sigma}{T_x}\right) - 1}. \quad (5)$$

With the solutions of Equations (3) and (4), the gain and the drift are calculated from Equations (6) and (7).

$$K(\sigma) = \frac{S_H^{Measured}(\sigma) - S_C^{Measured}(\sigma)}{L_H(\sigma) - L_C(\sigma)}, \quad (6)$$

$$M^{Stray}(\sigma) = \frac{L_H(\sigma)S_C^{Measured}(\sigma) - L_C(\sigma)S_H^{Measured}(\sigma)}{S_H^{Measured}(\sigma) - S_C^{Measured}(\sigma)}. \quad (7)$$

The calibrated spectrum is then given by Equation (8).

$$S^{Calibrated}(\sigma) = S^{Measured}(\sigma)K^{-1}(\sigma) - M^{Stray}(\sigma). \quad (8)$$

This calibration approach requires that the configurations of the instrument in use are the same as in calibration. All of the spectral information is included in the real part of the complex spectrum. The imaginary part contains only noise.

3.3 Calibration

The blackbody used in this study was the ZWK series blackbody from Shanghai Institute of Technology and Physics. The standard blackbody temperatures were set at 200°C, 500°C, 800°C, and 950°C, respectively. For each of them, measurements were taken when the temperature was stabilized for calibration. However, only one set of measurements was made in this study because the time was too long to stabilize the temperature (about 2 hours). Calibration was performed with this data set. A calibration file was generated. This file was used to calculate irradiances and

temperatures during the experiments.

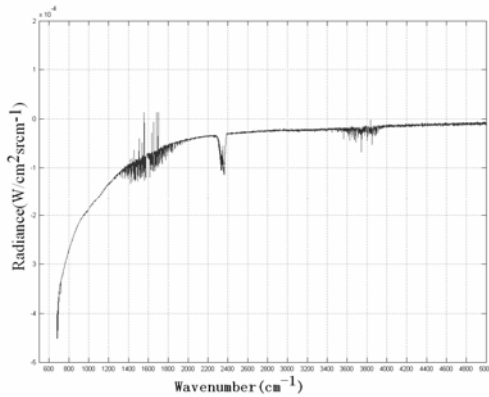


Figure 2 Spectrum of background target, night of October 20th, 2005.

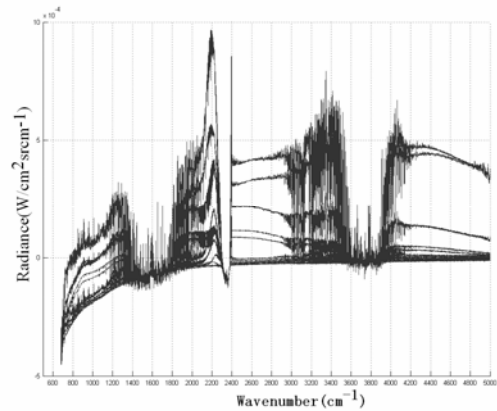


Figure 3 The spectra during the whole burning period, night of October 20th, 2005.

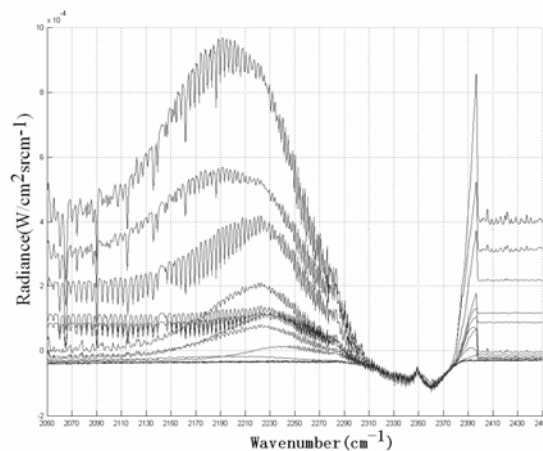


Figure 4 The medium wave spectrums in different burning phases, night of October 20th, 2005.

4. MEASUREMENTS AND SPECTRAL CHARACTERISTICS

4.1 Synchronous observations with the Satellite TERRA in the night of October 20th

The area of the fire was 100 m² (radius: 5.64 m). Fire setup is shown in Figure 1. The satellite EOS-TERRA passed over at 23:04 Beijing time. The fire was lighted at 22:30. Measurements of background radiation were taken before lighting. The results are shown in Figure 2. Spectral measurements were performed as described in the previous section. Figure 3 shows the spectra (650-5000cm⁻¹) during the whole burning period. The burning began with a weak fire, went to a strong one, and returned back to a weak fire at the end. Medium wave spectra in several different phases (2050-3450cm⁻¹) are shown in Figure 4.

4.2 Synchronous observations with the satellite FY-1D in the night of October 23rd

The area of this fire was 200 m² (radius: 7.98 m). The setup of the burning materials was the same as before. The fire

was lighted at 19:44 Beijing time. It reached the peak at 19:51, and then slightly weakened at 19:56. Satellite FY-1D passed over the field at 19:59 while the fire was in a good status. This experiment was very successful. The effects of raised temperature due to the fire were clearly reflected from the FY-1D satellite image. This fire spot was also identified in the MODIS global fire monitoring system⁵. Spectral irradiances are shown in Figure 5, while Figure 6 gives the spectra in middle wavelengths. Figure 7 depicts the spectral irradiances when the fire was at the strongest burning state.

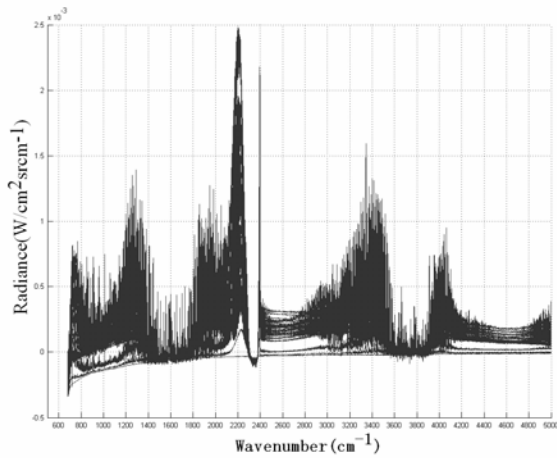


Figure 5 The total spectra during the whole burning period, October 23rd, 2005.

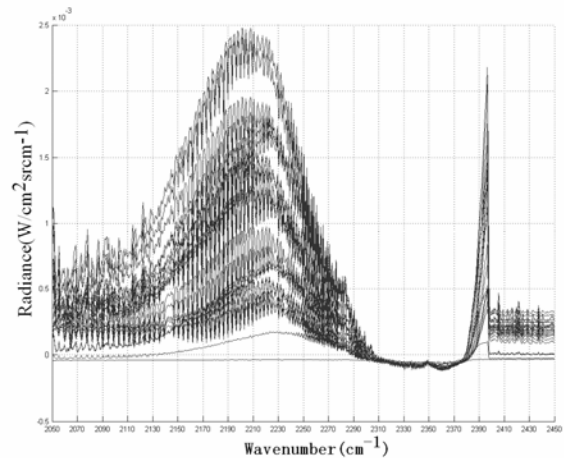


Figure 6 Spectra at middle wavelengths in different burning phases, October 23rd, 2005.

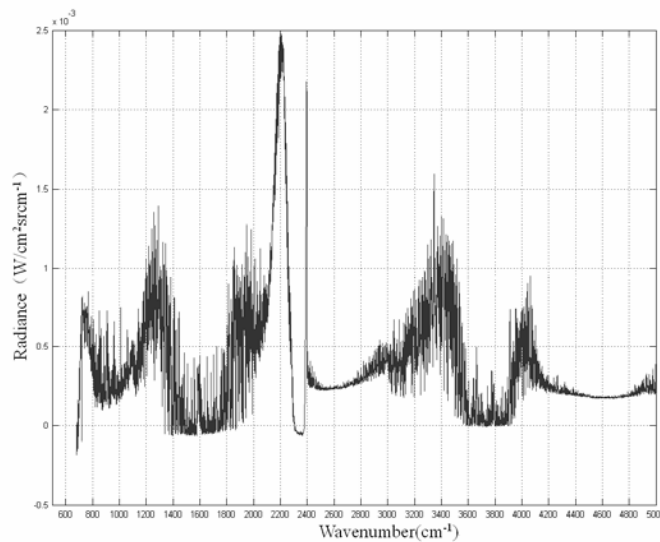


Figure 7 The infrared spectrum in the phase when the fire was in the strongest burning state, October 23rd, 2005.

4.3 Synchronous observations with the satellites EOS-TERRA and NOAA-17 on October 28th

This fire was set up the same as on October 23rd. Satellite EOS-TERRA passed over at 11:20 and NOAA-17 passed over at 11:31 Beijing time. To give a consideration to the passing times of these two satellites, the fire was lighted at 11:05

and it reached the peak at 11:14. The fire had weakened slightly since 11:18 and it was in the good burning status when satellite TERRA passed over the field. A clear increase in temperature was observed by the satellite. However, the fire was almost ceased while the NOAA-17 satellite was passing over and the observed temperature increase was not significant. Samples of spectral measurements at middle wavelengths in several burning phases are shown in Figure 8 and the spectral measurements when the fire was in the strongest burning state are given in Figure 9.

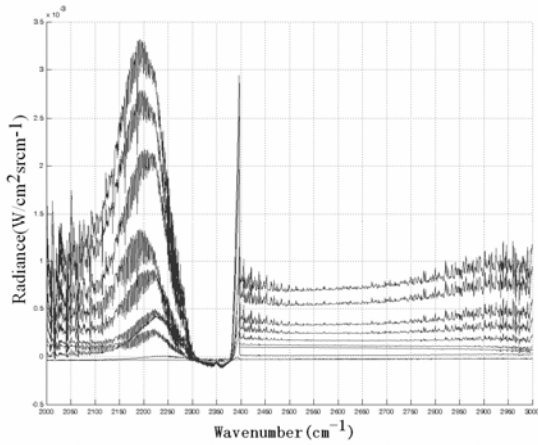


Figure 8 Spectral measurements at middle wavelengths sampled in different burning phases, October 28th, 2005.

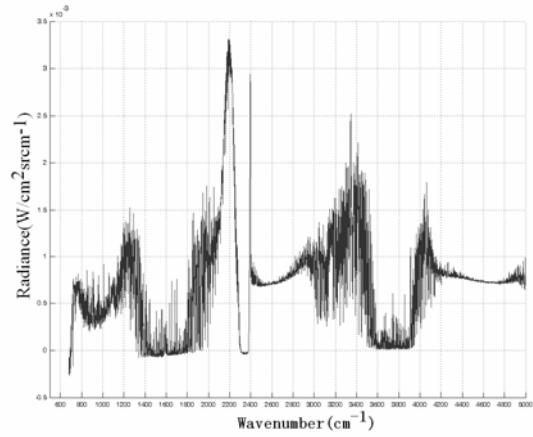


Figure 9 Spectral measurements at the strongest burning state, October 28th, 2005.

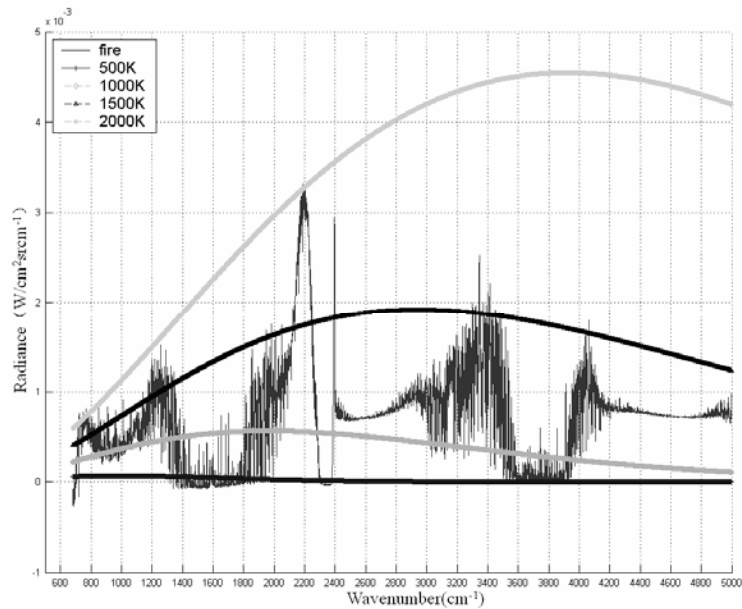


Figure 10 The radiation spectrum convolved with spectra of Plank functions at different temperatures.

4.4 Characteristics of the spectra and their application prospects

By analyzing the spectral measurements presented in Figures 2-9 we find strong correspondences of spectral irradiances at the middle infrared wavelengths, 4.34-4.76 μ m, with the burning process. Figure 10 convolves the spectrum of the fire

with the spectra of Plank functions at different temperatures. From this figure, the following characteristics of the spectra can be concluded.

- The left peak is located within $2190\text{-}2210\text{cm}^{-1}$ ($4.566\text{-}4.525\mu\text{m}$) and is generally in the wave band of $4.34\text{-}4.76\mu\text{m}$. This peak cannot be represented by the temperature characteristic of Plank function although it reflects the radiative feature of the fire.
- The right peak is located within $2378\text{-}2398\text{cm}^{-1}$ with a spike at 2396.4cm^{-1} ($4.17\mu\text{m}$) and its location never changes. It corresponds to the CO emission peak.⁶
- The medium wave band ($3.5\text{-}4.0\mu\text{m}$), which is commonly used in fire monitoring, is not in the wave peak, and its location drifts with the variation of fire intensity.
- The background CO₂ absorption peak is at 2360cm^{-1} ($4.237\mu\text{m}$).

Atmospheric transmission and radiative spectra were calculated from the observed optical depths and the atmospheric sounding data. Incident radiation was computed by extrapolating the fire spectra up to the atmospheric top using a numerical model. Figure 11 shows the atmospheric transmissivity spectrum over the experimental site on October 28, 2005 from the simultaneous sounding data. Comparisons between the ground fire spectra and the incident radiation spectra at the atmospheric top are presented in Figure 12. The following can be concluded from these figures.

- The maximum transmissivity was only 50% from the chosen channel since the water vapor content in the atmosphere was very high when the data was collected. However, the transmissivity at the middle infrared channel ($3.5\text{-}4.0\mu\text{m}$) could reach up to 90% under normal condition at the experimental site.
- The radiance of the fires from the chosen channel was five times brighter than the commonly used medium wavelength band and was three times stronger when it reached the satellite although its transmissivity was very low. This result suggests that this wavelength band can be used for fire monitoring. This band responds strongly to the fire burning and it responds to fires of much weaker than in the experiment and fires with smaller burning areas. To the remote sensing detectors, this implies a higher ratio of equivalent effective noise to the spectrum. An object can have a smaller angle of view for a satellite at the same height to observe (higher resolution).⁷A fire can be detected earlier when it is at the beginning.
- The wavelength band of $4.34\text{-}4.76\mu\text{m}$ facilitates to enhance the sensor's sensitivity and improve its spatial resolution since it is wide enough.

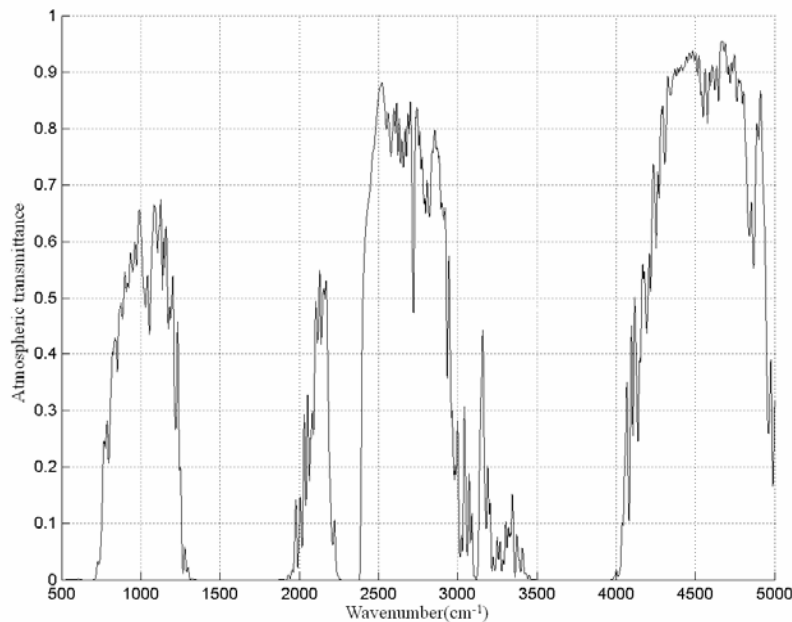


Figure 12 The atmospheric transmissivity spectrum over the experimental site on October 28th, 2005.

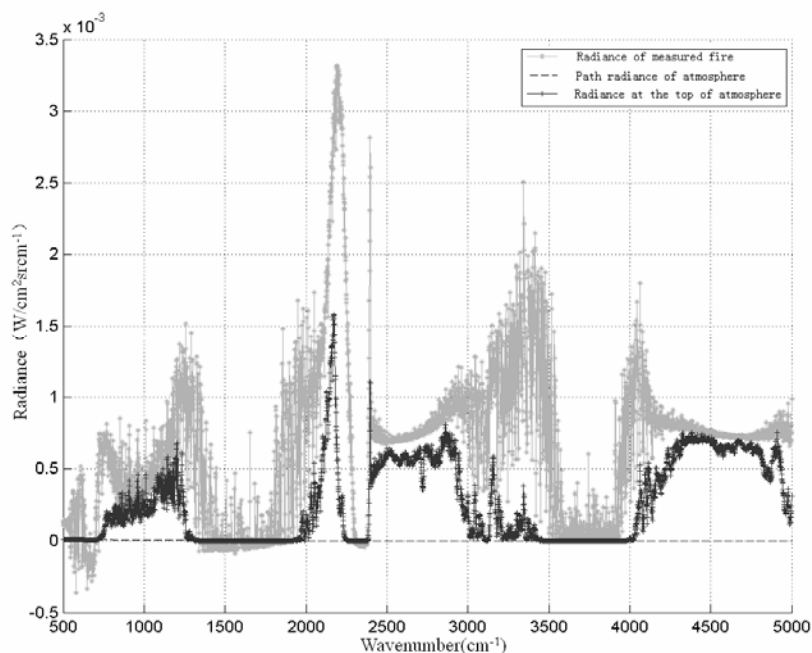


Figure 13 The ground-measured fire spectrum and the incident radiation spectrum from the satellite, October 28th, 2005.

5. CONCLUSION AND FUTURE WORK

Experiments with man-made fires were performed in a forest at Wuming county, Guangxi province in October 2005 to verify satellite remote sensing products for wild fire warning and to find more effective radiation channels for generating these products. Pine branches and trunks as well as other woody materials were burned in the experiments while satellites were passing over. These fires simulated forest fires well. Infrared spectra, temperature fields, and radiances were measured synchronously with the satellite data. Preliminary results have been presented in this paper.

Through data analysis we have found that two peaks can be identified in the near infrared spectral irradiance of the fires. One was located at $4.17\mu\text{m}$, reflecting the CO emission peak, and the other was within $4.34\text{--}4.76\mu\text{m}$, which was much stronger than the commonly used channel within the wavelengths of $3.5\text{--}4.0\mu\text{m}$ for fire monitoring. This finding suggests that the wavelengths of $4.34\text{--}4.76\mu\text{m}$ may be more suitable for wild fire monitoring using satellite data. This is a good reference for the development of sensors for wild fire detection.

Channel selection for fire monitoring is very complex. It involves works in various aspects. Further studies, analysis, and computations are necessary to further evaluate and verify our conclusions in the future.

ACKNOWLEDGEMENT

This work was funded by the Station Experiment Program of National Satellite Meteorological Center and was jointly supported by USDA UV-B Monitoring and Research Program under a grant from USDA CSREES 2005-34263-14270.

REFERENCE

1. Dozier, J., "A method for satellite identification of surface temperature fields of subpixel resolution", *Remote Sens. Environ.*, **11**, 221-229, 1981.
2. Flasse, S. P., and P. Ceccato, "A contextual algorithm for AVHRR fire detection", *Int. J. Remote Sens.*, **17**, 419-424, 1996.
3. Cheng Liu, "A sub-pixel method for estimating the area of fire spots and temperature using meteorological satellite data and its application", *Quarterly Journal of Applied Meteorology*, **15(3)**, 273-280, 2004.
4. Li, Z., Y. J. Kaufman, C. Ithoku, R. Fraser, A. Trishchenko, L. Giglio, J. Jin, and X. Yu, "A review of

- AVHRR-based active fire detection algorithms: Principles, limitations, and recommendations”, *Global and Regional Vegetation Fire Monitoring From Space, Planning and Coordinated International Effort*, F. Ahern, J. G. Goldammer, and C. Justice (eds), SPB Acad., The Hague, pp. 199-225, 2001.
5. Pereira, A. C., and A. W. Setzer, “Comparison of fire detection in savannas using AVHRR’s channel 3 and TM images”, *Int. J. Remote Sens.*, **17**, 1925-1937, 1996.
 6. Hao, W. M., D. E. Ward, G. Olbu, and S. P. Baker, “Emissions of CO₂, CO, and hydrocarbons from fires in diverse African savanna ecosystems”, *J. Geophys. Res.*, **101**, 23,577-23,584, 1996.
 7. Gutman, G., C. D. Elvidge, I. Csiszar, and P. Romanov, “NOAA archive of data from meteorological satellite useful for fire product”, *Global and Regional Vegetation Fire Monitoring From Space: Planning and Coordinated International Effort*, F. Ahern, J. G. Goldammer, and C. Justice (eds), SPB Acad., The Hague, Netherlands, pp. 257-265, 2001.